


<p>C. Jaipradidtham</p>	<h1>Wavelet Transform-Signal Processing for Fault Detection in 500 kV EHV Transmission Lines of Power System Using Genetic Algorithm</h1>	
-------------------------	---	---

Abstract- This paper presents the use of wavelet transform for analyzing power system fault detection in order to determine the fault location and the fault phase selection in 500 kV double circuit transmission lines of type DL3° and DT20° using genetic algorithms. The wavelet transform (WT) has been successfully applied in many fields. The technique is based on using the absolute sum value of coefficients in multiresolution signal decomposition based on the discrete wavelet transform (DWT). By performing the simulation of fault signal and parameter adjustments, with have effect with ATP/EMTP program. The result of experiment shows that can indicate the specify fault location, fault classification, phase selection and fault circuit transmission line. The simulation of the 500 kV power system using EMTP program were used to test the performance of the simple genetic algorithms.

Keywords – Power system, wavelet transform, genetic algorithm, and transients analysis.

Chamni Jaipradidtham is with Dept. of Electrical Engineering , Faculty of Engineering , Kasem Bundit University, Bangkok 10250, Thailand , He can be reached at E-mail: j_chamni@hotmail.com

I. INTRODUCTION

Transmission line system for fault location has long been one of the primary concerns of the power industry. Simulation of transients along 500 kV system can be best performed in the frequency domain, since the line parameters are known to vary significantly as a function of frequency, and the other utilizing the high frequency contents of the transient fault signals. The latter is also referred to as traveling wave. The use of traveling wave theory for fault detection was initially proposed, reliable phase selection of the faulted phase is very important in order to avoid unnecessary three-phase tripping or alternatively tripping of the incorrect phase. Wavelet transforms with their ability to focus on short transients and high frequency components can provide an effective solution to the accurate phase selection. This paper presents a technique for fault location and phase selection by wavelet transform (WT) of genetic algorithms (GA). Genetic algorithms have shown a rapid growth of applications in power system. A wavelet based technique for power system transients analysis was simulated using the ATP/EMTP program.

II. THE ANALYSIS

A. Structures of 500 kV Transmission lines

The following are the assumed characteristic of the line for which outage rate performance will be determined is given by:

- Conductor : 4 Bundle per phase x 795 MCM : 54/7
 Spacing between = 45.7 cm
 Diameter = 2.773 cm
 Ruling span = 420 m
 Ultimate strength = 12,800 kg
 Weight = 1.52 kg/m
 Wind span = 500 m
- Shield wire: 3/8" EHS, Class A, Galvanized steel
 Number of wires = 2 per tower
 Shielding angle = -5° to outer phases
 Ultimate strength = 6985 kg
 Diameter = 9.1444 mm
 Weight = 0.406 kg/m
- Insulator : Type Suspension, ball and socket
 ANSI Class 52-8 and ANSI Class 52-11
 Based on max. conductor tension of 22%
 rated tensile strength with wind pressure
- Grounding system : ground resistance 10 ohms or less
 A. Stub angle to rebar : used in all cases
 B. Ground rods : used in all cases,
- Lightning outage rate : Less than 0.05 /100 km/ year
 Right-of-way width : 70 meters for each line.

The method is to be envisioned in the following 4 stages :

- Establishing the flashover probability in number of tower and the tower top voltage.
- Establishing the critical stroke current and the Gaussian frequency.

- Establishing the probability of back-flashover as a function of line configuration, footing resistance, CFO for a random stroke to the tower.
- Establishing the extreme value distribution and line back-flashover outage rate.

B. Discrete Wavelet Transform

Wavelet analysis is a recently developed mathematical tool for signal analysis. Wavelet transforms are based on a set of signal derived from a basic mother wavelet by adjusting the time-shifting and dilation parameters[1]. Discrete wavelet transform (DWT) is derived from a continuous wavelet transform (CWT). The CWT has a digitally implementable counterpart known as the DWT become as:

$$DWT(m,k) = \frac{1}{\sqrt{a_0^m}} \sum_{n=-\infty}^{+\infty} x(n)g\left(\frac{k - nb_0 a_0^m}{a_0^m}\right) \quad (1)$$

where

$x(n)$ is the discretized signal function

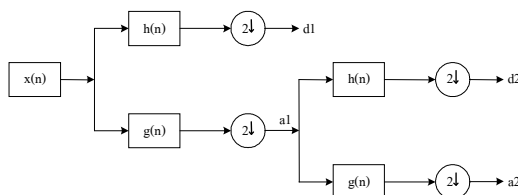
This scaling gives the DWT a logarithmic frequency coverage and this is in marked contrast to the uniform frequency coverage. By simple interchange of the variables n, k and rearrangement of the DWT gives[2].

$$DWT(m,n) = \frac{1}{\sqrt{a_0^m}} \sum_k x(k)g(a_0^{-m}n - b_0k) \quad (2)$$

DWT can be easily and quickly implemented by filter bank techniques if the coefficients are thought of as a filter as shown in (3)

$$DWT(m,n) = C(i,j) = \sum_{n=0}^{N-1} x(n)2^{-j/2}g(2^i n - j) \quad (3)$$

The implementation of the DWT with a filter bank is computationally efficient. The output of the high-pass filter (HPF) gives the detailed version of the high-frequency component of the signal is shown in Fig.1 [3] where $x(n)$ is the original signal, $h(n)$ and $g(n)$ are high-pass and low-pass filter (LPF), respectively. $(2\downarrow)$ represents down sampling of the input signal, $a1$ and $d1$ represent approximations and details at first scale.



$g(n)$ is the mother wavelet
 a and b are functions of integer parameter m

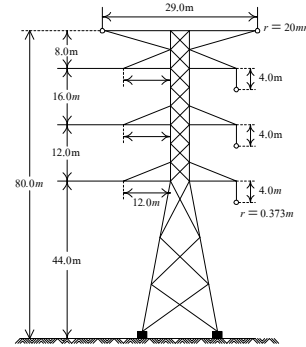


Fig. 2 : Structures characteristic of 500 kV double Circuit transmission lines of type DT20

Fig. 1: Wavelet decomposition tree

C. Fault Location and Phase Selection

When the fault involves a connection to ground, then sending end signal may contain significant reflections from the remote end bus in addition to the ones from the fault point. The actual fault location can be accurately identified by the following formula [3]:

$$D_m = \frac{\ln\left(\frac{N_m}{M_m}\right)}{2\Gamma_m L} ; m = 0, \alpha, \beta \quad (4)$$

where

- N_m is equal to zero too and at zero before fault.
- M_m is the modal fault detection and the values of M_m are equal to 1 before the fault is detected.
- Γ_m is represent modal propagation constant
- L is the total length of the protected line

And then the modified modal fault detection indices are defined as:

$$|M_m| = \frac{|M_m|}{|M_m|_{prefault}} \quad (5)$$

where

$|M_m|_{prefault}$ is the last offset value before the fault is detected.

Type of fault is AG, BG, CG, ABG, BCG, CAG, AB, BC, CA and ABC

Fault location is 10% -90% of all distance
 Load size is 500 MVA (pf. =0.8)
 Fault angles is 0°, 30°, 60°, 90°, 120°, 150°, 180°, 210°, 240°, 270°, 300°, 330°

The fault detection process by using the wavelet transform technique. The WT detection technique provides the ability to detect the disturbance occurring in the related phase. The fault classification and phase selection cannot be achieved directly from the pattern listed (phase A ,phase B and phase C).

D. Genetic Algorithms Construction

A genetic algorithms(GA) may solve these kinds of complex problems. This is the option to increase redundancy in the components. The objective function is to determine the number of components in parallel where reliability is maximized subject to restrictions. The problem for load point reliability optimization is discrete, as transmission lines in parallel are added to the power system[4]. The inputs to the system are probabilistic distributions for the transmission lines failure rates[5]. Application of genetic algorithm to power system is found in areas such as economic dispatch, power system planning, reactive power allocation and the power load flow problem. Genetic algorithm are appropriate for stochastic and large-scale problems with nonlinearities. They satisfy the design requirements for reliability problems. The first one is the selection from parents and the second one is applying the crossover operator . Selection procedures are as follows.

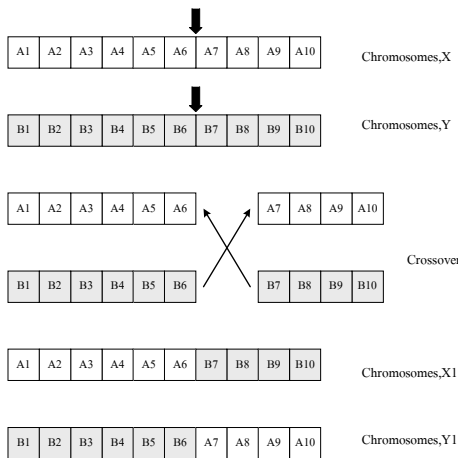


Fig.3 : Crossover of A and B chromosomes

Step 1) Calculate the total fitness of the population

$$F = \sum_{i=1}^{pop_size} Fit_i \tag{6}$$

Step 2) Calculate the probability of a selection for each chromosome *i*.

$$ps_i = \frac{Fit_i}{F} \tag{7}$$

The fitness of the chromosome can be calculated as

$$Fit_i = copy_i \cdot P_i \text{ or } Fit_i = P_i \tag{8}$$

Step 3) Calculate the cumulative probability *q_i* for each chromosome “ *i* ” by adding its selection probability to those of all previous “ *i - 1* ” chromosomes in the current population.

$$q_i = \sum_{j=1}^i ps_j \tag{9}$$

Step 4) The selection process is based on spinning the roulette wheel *pop_size* times. Where input parameters are *pop_size*. A single chromosome is selected for the new population each time.

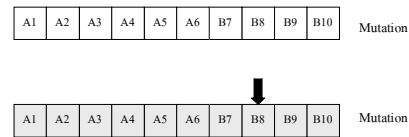


Fig. 4: Crossover and Mutation

Step 5) Generate a random number *r* from the range [0,...,1]. If *r* < *q_i*, then select the first chromosome;

otherwise select the *i*th one such that *q_{i-1}* < *r* ≤ *q_i*.

Step 6) In this manner, the some chromosomes are selected more than once. The best chromosomes get more copies; the average stay even and the worst off.

E. Model Transmission Line System

The model system used in the study is the simplified double circuit transmission line as illustrated in Fig.5. The transmission line is a 500 kV. The first section AB contains two 325 km long parallel lines, and the second section BC is equivalent to a 100 km line. It is able to transmit the power from the Mae Moh3(MM3) power plant in Lampang Province to substation plant at Tha Tako(TTK) in Nakornswan province. Each of the parallel lines has a zero sequence impedance is *Z₀* = 84.21+ j 325.6 ohms; and positive sequence impedance is *Z_p* = 7.65+ j 120.92 ohms.

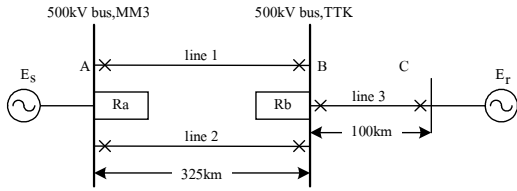


Fig.5: Parallel transmission line model of the simulated

III. SIMULATION RESULTS

The simulation results have been carried out based on using ATP/EMTP program simulator. This paper a novel technique for phase selection using wavelet transforms. The 3-phase transmission system consists of double circuit of type DL3° and DT20°. The configuration of the lines are shown in Fig.5. The selected fault inception angles were 90°, 180°, 270° and 360° from phase A. Fault locations were varied in steps of 15 % of line length. In Fig. 6 show the frequency spectrum of phase voltages just after fault inception for a ground fault at different fault locations. The wavelet transform coefficient of a phase to ground fault at 40 miles from bus A. The DWT result of differential current calculated by using measured primary and secondary currents in phase A, B and C for the incipient behavior are given in Fig.7 and Fig.9.

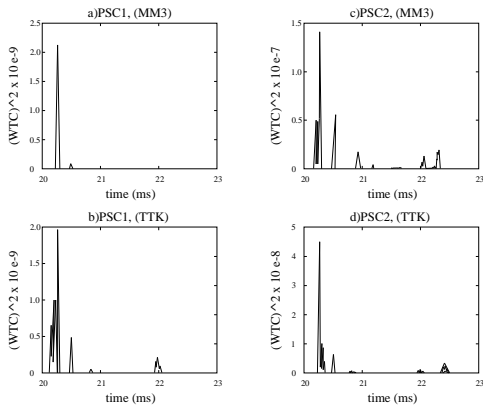


Fig. 6: Phase to ground fault at 40 miles at bus A

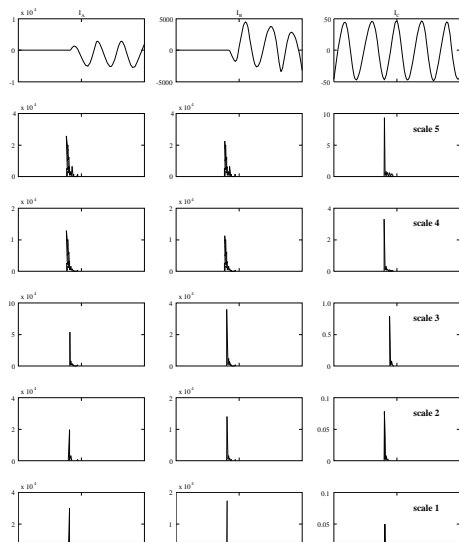


Fig. 7: Wavelet transforms of 2 phase to ground fault; case for fault circuit 1

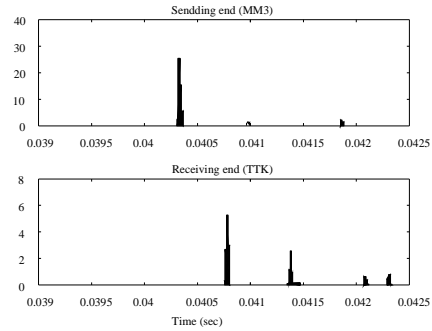


Fig. 8: Fault current signal for differential components

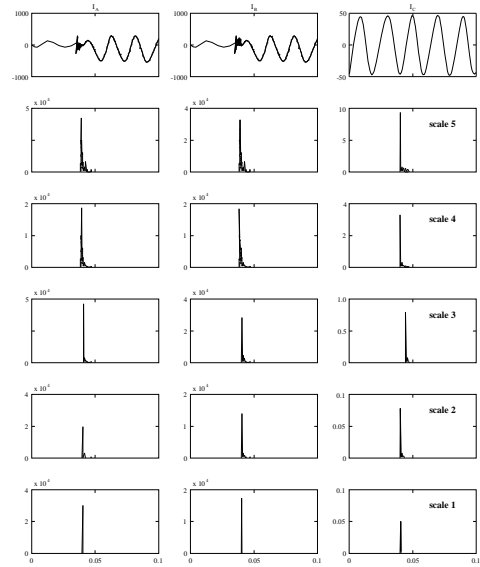


Fig. 9: Wavelet transforms of 2 phase to ground fault ; case for fault circuit 2

IV. CONCLUSION

This paper has presented the application of wavelet transform for distance protection of 500 kV EHV transmission lines by using genetic algorithm. The WCT at the two lowest scales are then used to determine the fault location for various types of faults and line configurations. The fault location estimation error is less than 1% to the sampling time used in recording the fault transient and high frequency components of the fault signals can provide an effective solution to the accurate phase selection problem. The results show that the proposed method provides high accuracy of fault type identifications and can be applied as a part of high speed protective relays.

V. ACKNOWLEDGMENT

The authors acknowledge gratefully the support provided by Kasem Bundit University, Thailand, for this work and the research work in this paper is jointly sponsored by program of University.

VI. REFERENCES

- [1] Joe-Air Jiang and et.al., "A New Protection Scheme for Fault Detection, Classification and Location in Transmission Lines," *IEEE Trans. on Power Deliv.*, vol.18, No.1, pp.34-42, January 2003.
- [2] Karen L. Butler-Purry and M. Bagriyanik, "Characterization of Transients in Transformers using Discrete Wavelet Transforms," *IEEE Trans. on Power System*, vol.18, No.2, pp. 648-656, May 2003.
- [3] Chul-Hwan Kin and et.al., "A Novel Fault Detection Technique of High Impedance Arcing Faults in Transmission Lines using the Wavelet Transform," *IEEE Trans. on Power Deliv.*, vol.17, No.4, pp.921-929, Oct 2002.
- [4] D. Romero and J.A. Gomez-Hernandez, "Transmission Reliability Optimization Utilizing a Genetic Algorithm," *Inter. Journal of Power and Energy System*, pp.34-42, 2002.
- [5] Nader, S. and Chanan, S., "Adequacy Assessment of Power System Generation using a Modified Simple Genetic Algorithm," *IEEE Trans. on Power System*, pp.974-981, 2002.
- [6] V.L. Pham and K.P. Wong, "Wavelet-transform-based algorithm for harmonic analysis of power system waveforms," *IEE Proc. - Gener. Transm. Distrib.*, vol.146, pp.249-254, 1999.
- [7] Dong-Jiang Zhang, Q. Henry Wu and et al., "Transient positional protection of transmission lines using complex wavelet analysis" *IEEE Trans. Power Delivery*, vol.18, pp.705-710, July 2003.
- [8] H. Xue and R. Yang, "Optimal interpolating windowed discrete fourier transform algorithms for harmonic analysis in power systems," *IEE Proc. -Gener. Transm. Distrib.*, vol.150, pp.583-587, September 2003.
- [9] A.H. Osman and O.P. Malik, "Transmission line distance protection based on wavelet transform," *IEEE Trans. Power Delivery*, vol.19, pp.515-523, April 2004.
- [10] V.L. Pham and K.P. Wong, "Antidistortion method for wavelet transform filter banks and nonstationary power system waveform harmonics analysis," *IEE Proc. - Gener. Transm. Distrib.*, vol.148, pp.117-122, March 2001.
- [11] P. Chowdhuri, S. Li and P. Yan, "Review of research on lightning induced voltages on an overhead line," *IEE Proc. -Gener. Trans. Distrib.*, vol.148, pp.91-95, January. 2001.
- [12] R. Moini, V. A. Rakov, M. A. Uman, B. Kordi, "An antenna theory model for the lightning return stroke", 12th Intern. Zurich Symp., and Technical Exhibition on EMC system, February 18-20, 1997.
- [13] P. Chowdhuri, "Estimation of flashover rates of overhead power distribution lines by lightning strokes to nearby ground," *IEEE*

Trans. on Power Delivery, vol.4, no. 3, pp.1982-1989, July 1989.

- [14] J.A. Martinez, F. Gonzalez, "Statistical evaluation of lightning overvoltages on overhead distribution transmission line using neural network", *IEEE PES 2001*, pp.1133-1138, 2004.
- [15] Brown, G.W., "Designing EHV lines to a given outage rate simplified," *IEEE Trans. on Power Systems*, 2001.
- [16] EGAT, "Contract documents of 500 kV transmission line Mae Moh3 -Tha-Tako", Bangkok, September, 1983.

VII. BIOGRAPHIES

Chamni Jaipradidtham received M. Eng. degree in Electrical Engineering from KMITL, Bangkok, Thailand. His research interests are harmonic analysis, energy & power system, high voltage engineering and electrical machines. He is a lecturer at Department of Electrical Engineering, Faculty of Engineering at the Kasem Bundit University.



¹P. Kumar
²V. Agarwal

Tuning of PI Controller for Current Source Inverter Fed Induction Motor Drive



Abstract— Direct torque control (DTC) of Induction motor is preferred as compared to vector control scheme due to its quick torque response, simplicity and robustness against rotor parameters variation. PID controllers are very common since they can offer a satisfactory performance over a wide range of operation. The main problem with this controller is the correct choice of the PID gains and the fact that by using fixed gains, the controller may not provide the required control performance, when there are variations in the plant parameters and operating conditions. Therefore, a tuning process must be performed to ensure that the controller can deal with the variations in the plant. The tuning of these controllers is governed by system nonlinearities and continuous parameter variations. In this paper, a complete and rigorous study is made for tuning of PI controller used in a speed control loop in a Direct Torque Control (DTC) scheme applied in a current source inverter (CSI) fed induction motor drive system. The controller value is adjusted by Ziegler and Nichols method. A comparative study is made between P and PI controller. It has been found that with P controller the transient time to reach the steady state value is small.

Keywords – Direct torque control, current source inverter, Ziegler and Nichols

Nomenclature

v_{as}, v_{bs}, v_{cs}	= Stator phase voltages
v_{qs}, v_{ds}	= Stator phase voltages in d-q reference frame
v_{qr}, v_{dr}	= Rotor phase voltages in d-q reference frame
i_a, i_b, i_c	= Inverter output currents
i_q, i_d	= Inverter output currents in d-q reference frame
i_{as}, i_{bs}, i_{cs}	= Stator currents
i_{qs}, i_{ds}	= Stator currents in d-q reference frame
i_{qr}, i_{dr}	= Rotor currents in d-q reference frame
i_{act}, i_{react}	= Active & reactive component of stator current
i_{ref}, i_c	= Reference current, Capacitor current
ω_e	= Electrical angular velocity of d-q axis
ω_r	= Electrical angular velocity of rotor
ω_{sl}	= Slip speed in rad/sec
ω_{slref}	= Slip speed command in rad/sec
T_e, T_l	= Electromagnetic torque and load torque
v_{dc}, i_{dc}	= Rectifier output voltage, DC link current
v_i	= Inverter input voltage
v_s, v_r	= Amplitude of stator & rotor voltage
r_s, r_r	= Stator & rotor resistance
l_s, l_r	= Stator & rotor self inductance

l_m	= Mutual inductance between stator and rotor
C	= Capacitance of each output capacitor
r_f, l_f	= DC link resistance & inductance
P	= Number of pole
J	= Moment of inertia of rotor 'Kg-m ² '
K_{ps}	= Proportional gain of speed controller
K_{pi}	= Proportional gain of current controller
K_1, K_2	= Slope of active & reactive component of slip regulator characteristics respectively

I. INTRODUCTION

The speed of an induction motor can be smoothly controlled over a desired speed range by varying the frequency of AC source. Due to inherent disadvantages in voltage source inverter [1], a slip regulated current source inverter (CSI) has been preferred for a wide range speed control [2, 3]. The current source inverter fed drive finds application in high power drives such as fan drives, where fast dynamic response is not needed. Also, since CSI drives employ fully controlled silicon-controlled rectifier (SCR) converter at the input. Under regeneration the polarity of the voltage at the converter terminals will reverse and the energy will be fed back to the utility. So regeneration is built in to the system and unlike VSI fed drives does not require any additional circuit [4]. In CSI drives the dc link reactor limits the rate of rise of current under short circuit conditions, so the drives can be easily protected under short circuit and thus results in improved reliability of the drive [5, 6].

The most common choice for the controller in CSI drive is the PID compensator due to its simple structure and satisfactory performance over a wide range of operation [7]. To tune a PI controller (usually in drives applications the derivative part of the controller is not used) [8] a lot of strategies have been proposed.. The technique [9] uses

¹Piush Kumar is currently the Research Scholar of Electrical Engineering, Motilal Nehru National Institute of Technology Allahabad, India. He can be reached at: piushgg@yahoo.com.

²Vineeta Agarwal is currently the Faculty of Electrical Engineering, Motilal Nehru National Institute of Technology Allahabad, India. She can be reached at: vineeta_agarwal123@rediffmail.com.

frequency response method to design and tune PI controller gains based on specified phase and gain margins as well as cross over frequency. Furthermore, root locus and pole assignment design techniques are also proposed in addition to transient response specifications. All these methods are considered as model based strategies and then the efficiency of the tuning law depends on the accuracy of the proposed model as well as the assumed conditions with respect to actual operating conditions [10, 11]. On the other hand the Ziegler-Nichols method does not require any system model and control parameters are designed only from the plant step response [12]. Tuning, using this method is characterized by a good disturbance rejection. This paper presents tuning of PI Controller for Current Source Inverter Fed Induction Motor Drive. In this study, the dynamic analysis of SCCSI fed induction motor system is done with proportional and integral controller in speed and current loops, the parameter of which are adjusted by Ziegler and Nichols method. Simulation studies are made at various motor speeds for different loading conditions. It has been shown that due to very small offset, P controller works satisfactorily as compared to PI controller for all loads.

II. CSI FED IM DRIVE SYSTEM

Fig. 1 shows a current controlled induction motor drive system. It consists of three phase power source, controlled rectifier bridge, a DC link smoothing reactor, a current source inverter and a three phase squirrel cage induction motor. The magnitude and polarity of the speed error are used to determine the slip speed reference. This maintains the air gap flux in the machine at a constant value and also used to determine the DC link current reference value. Rectifier output voltage is controlled by PI controller working on the DC link current error that decides the input current of CSI. The slip speed is added to the rotor speed in order to determine the synchronous speed, which then determines the inverter operating frequency.

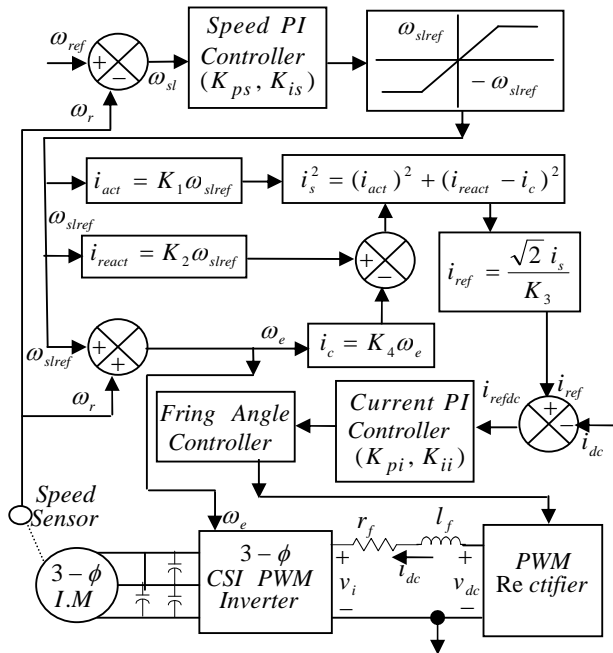


Fig. 1. Closed Loop Control of Induction Motor fed by CSI

III. MODELING OF CSI FED IM DRIVE SYSTEM

The composite inverter fed induction motor system has been modeled in different structures and cascaded together to obtain the overall performance of system.

A. Modeling of Induction Motor

The voltages and currents of the squirrel cage induction motor can be represented in a synchronously rotating d-q reference frame as follows [13]

$$\begin{bmatrix} v_{qs} \\ v_{ds} \\ v_{qr} \\ v_{dr} \end{bmatrix} = \begin{bmatrix} r_s + pl_s & \omega_e l_s & pl_m & \omega_e l_m \\ -\omega_e l_s & r_s + pl_s & -\omega_e l_m & pl_m \\ pl_m & \omega_{sl} l_m & r_r + pl_r & \omega_{sl} l_r \\ -\omega_{sl} l_m & pl_m & -\omega_{sl} l_r & r_r + pl_r \end{bmatrix} \begin{bmatrix} i_{qs} \\ i_{ds} \\ i_{qr} \\ i_{dr} \end{bmatrix} \quad (1)$$

Solving (1), following model of induction motor is obtained

$$\begin{bmatrix} \dot{i}_{ds} \\ \dot{i}_{qs} \\ \dot{i}_{dr} \\ \dot{i}_{qr} \end{bmatrix} = \frac{1}{l_1} \begin{bmatrix} -r_s l_r & \omega_l + \omega_l^2 l_m^2 & r_l l_m & \omega_l l_{lr} \\ -(\omega_l + \omega_l^2 l_m^2) & -r_s l_r & -\omega_l l_{lr} & r_l l_m \\ r_s l_m & -\omega_l l_{ms} & -r_l l_s & \omega_l - \omega_l l_{sr} \\ \omega_l l_{sm} & r_l l_m & -(\omega_l - \omega_l l_{sr}) & -r_l l_s \end{bmatrix} \begin{bmatrix} i_{ds} \\ i_{qs} \\ i_{dr} \\ i_{qr} \end{bmatrix} + \frac{1}{l_1} \begin{bmatrix} l_r & 0 & 0 & 0 \\ 0 & l_r & 0 & 0 \\ -l_m & 0 & 0 & 0 \\ 0 & -l_m & 0 & 0 \end{bmatrix} \begin{bmatrix} v_{ds} \\ v_{qs} \\ 0 \\ 0 \end{bmatrix} \quad (2)$$

$$\text{Where } l_1 = l_s l_r - l_m^2 \quad (3)$$

The machine and load torque are related as

$$Jp\omega_r = T_e - T_l \quad (4)$$

In equation (4), friction and windage losses are neglected. The electromagnetic torque, T_e and load torque, T_l is given by the following equations.

$$T_e = (3P/4)l_m (i_{qs} i_{dr} - i_{ds} i_{qr}) \quad (5)$$

$$T_l = T_L * (\omega_r / \omega_b) \quad (6)$$

The load torque in the present case is considered to be varying linearly with the speed.

B. Modeling of Capacitors

For the balanced condition, the equations related to the output capacitors can be expressed, in term of phase voltages as following:

$$i_a = 3Cp v_{as} + i_{as} \quad (7)$$

$$i_b = 3Cp v_{bs} + i_{bs} \quad (8)$$

$$i_c = 3Cp v_{cs} + i_{cs} \quad (9)$$

Transforming the inverter output currents i_a, i_b & i_c in a synchronously rotating d-q reference frame, following equations are obtained.

$$i_q = 3Cpv_{qs} + 3C\omega_e v_{ds} + i_{qs} \quad (10)$$

$$i_d = 3Cpv_{ds} - 3C\omega_e v_{qs} + i_{ds} \quad (11)$$

In CSI the inverter output current flows for 120° of each half cycle in the form of a rectangular wave. Their harmonic components are neglected on the assumptions that the drive system stability is primarily determined by the fundamental component of each variable. Thus, the inverter output currents, considering only the fundamental component, are obtained as below

$$i_q = (2\sqrt{3}/\pi)i_{dc}, \quad i_d = 0 \quad (12)$$

From equation (10) to (12) the derivative of stator phase voltage in dq reference frame are obtained

$$pv_{ds} = (1/3C)(-i_{ds} + 3C\omega_e v_{qs}) \quad (13)$$

$$pv_{qs} = (1/3C)(2\sqrt{2}/\pi)i_{dc} - 3C\omega_e v_{ds} - i_{qs} \quad (14)$$

C. Modeling of DC Link

The dc link is expressed as

$$l_f p i_{dc} + r_f i_{dc} = v_{dc} - v_i \quad (15)$$

If inverter is assumed lossless, the inverter input voltage be

$$v_i = (3\sqrt{3}/\pi)v_{qs} \quad (16)$$

The relationship between the stator rms current and dc reference current is

$$i_{ref} = (\sqrt{2}/K_3)i_s \quad (17)$$

IV. STEADY STATE CHARACTERISTICS

Tuning a controller involves setting the proportional, integral, and derivative values to get the best possible control for a particular process. In order to obtain the adequate control the motor is tuned here using Ziegler Nichols Method.

The test machine used in the work is a 3-phase, 400/440V, 50 Hz, 4 poles, 7 Amps, induction motor. Different parameters of the motor are $r_s = r_r = 5.53 \Omega/\text{ph}$, $l_s = l_r = 0.68 \text{ H}$, $l_m = 0.6503 \text{ H}$, $l_f = 0.05 \text{ H}$, $r_f = 3 \Omega$, $C = 28.22 \mu\text{F}$, $K_1 = 0.0821$ and $K_2 = 0.2474$.

The steady state equation (18) is obtained by substituting all the derivative terms equal to zero in the equations (1), (13) and (14) and assuming the DC link current i_{dc} as an input.

$$\begin{bmatrix} 0 \\ 0 \\ 0 \\ 0 \\ \frac{-2\sqrt{3}}{3C}i_{dc} \\ 0 \end{bmatrix} = \begin{bmatrix} -r_s & -(\omega l_1 + \omega l_m^2) & r_{lm} & -\omega l_{lm} & l_r & 0 \\ \omega l_1 + \omega l_m^2 & -r_{sr} & \omega l_{mr} & r_{lm} & 0 & l_r \\ l_{ms} & \omega l_{ms} & -r_{sr} & \omega l_{sr} - \omega l_1 & -l_m & 0 \\ -\omega l_{sm} & r_{sm} & \omega l_1 - \omega l_{rs} & -r_{sr} & 0 & -l_m \\ \frac{-l_1}{3C} & 0 & 0 & 0 & 0 & -l_1 \omega \\ 0 & 0 & \frac{-l_1}{3C} & 0 & 0 & l_1 \omega \end{bmatrix} \begin{bmatrix} i_{qo} \\ i_{do} \\ i_{qo} \\ i_{do} \\ v_{qo} \\ v_{do} \end{bmatrix} \quad (18)$$

The subscript 'o' denotes the steady state value. Once the DC link current required for an arbitrary speed and a load torque is determined, all the motor currents and the developed electromagnetic torque can be obtained using equations (18) and (5) respectively. Fig. 2 shows the torque versus slip characteristics for different value of dc link current. Near the synchronous speed i.e. at low slips the torque is linear and is proportional to slip; beyond the maximum torque the torque is approximately inversely proportional to slip. Fig.3 shows the rotor current characteristic for different value of dc link current. It shows that at unity slip the current taken by the motor is large as expected.

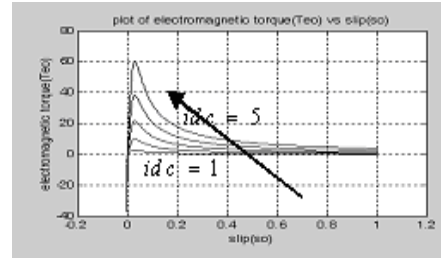


Fig. 2. Plot of electromagnetic torque (Te) vs slip(s)

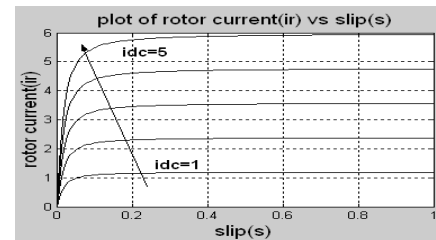


Fig. 3. Plot of rotor current (ir) vs slip(s)

V. DYNAMIC CHARACTERISTICS

To investigate the dynamic characteristics, the equations (1), (4), (5), (10), (11), (15) & (16) are linearized about a steady state operating point. Then the resulting state equation can be expressed as

$$\dot{x} = Ax + Bu \quad (19)$$

Where

$$x = [\delta i_{qs} \quad \delta i_{ds} \quad \delta i_{qr} \quad \delta i_{dr} \quad \delta v_{qs} \quad \delta v_{ds} \quad \delta i_{dc} \quad \delta \omega_r]^T \quad (20)$$

$$u = [\delta \omega_s \quad \delta v_{dc} \quad \delta T_l]^T \quad (21)$$

$$A = \frac{1}{l_1} \begin{bmatrix} -r_s l_r & l_m^2 \omega_{slo} - l_s l_r \omega_{so} & r_r l_m & -\omega_{ro} l_m l_r & l_r & 0 & 0 & -(l_m^2 i_{dso} + l_m l_r i_{dro}) \\ l_r l_s \omega_{so} - l_m^2 \omega_{slo} & -l_r l_s & l_r l_m \omega_{ro} & l_m l_r & 0 & l_r & 0 & (l_m^2 i_{qso} + l_m l_r i_{qro}) \\ r_s l_m & l_s l_m \omega_{ro} & -r_r l_s & l_m^2 \omega_{so} - l_s l_r \omega_{slo} & -l_m & 0 & 0 & (l_m i_{dso} + l_r i_{dro}) l_s \\ -l_s l_m \omega_{ro} & l_m r_s & -(l_m^2 \omega_{so} - l_r l_s \omega_{slo}) & -r_r l_s & 0 & -l_m & 0 & -(l_m i_{qso} + l_r i_{qro}) l_s \\ -\frac{l_1}{3C} & 0 & 0 & 0 & 0 & -l_1 \omega_{so} & \frac{2l_1}{\pi C \sqrt{3}} & 0 \\ 0 & -\frac{l_1}{3C} & 0 & 0 & l_1 \omega_{so} & 0 & 0 & 0 \\ 0 & 0 & 0 & 0 & \frac{3\sqrt{3}l_1}{\pi l_f} & 0 & -\frac{r_f l_1}{l_f} & 0 \\ \frac{3P^2 l_m l_1}{8J} i_{dro} & -\frac{3P^2 l_m l_1}{8J} i_{qro} & -\frac{3P^2 l_m l_1}{8J} i_{dso} & \frac{3P^2 l_m l_1}{8J} i_{qso} & 0 & 0 & 0 & 0 \end{bmatrix} \quad (22)$$

$$B = \frac{1}{l_1} \begin{bmatrix} -l_1 i_{dso} & 0 & 0 \\ l_1 i_{qso} & 0 & 0 \\ -l_1 i_{dro} & 0 & 0 \\ l_1 i_{qro} & 0 & 0 \\ -l_1 v_{dso} & 0 & 0 \\ l_1 v_{qso} & 0 & 0 \\ 0 & \frac{l_1}{l_f} & 0 \\ 0 & 0 & -\frac{P}{2J} \end{bmatrix} \quad (23)$$

Software MATLAB is used to solve Equation (19) to investigate the starting transient of the drive. Initially, load torque is kept at very low value equal to 0.8 N-M. In order to obtain the steady state operating value corresponding to this load torque, the dC link current range has been obtained with the help of steady state characteristic shown in Fig.2. To obtain high efficiency it is preferred to operate near low slips. Now the controller gain is adjusted when speed was taken equal to $\omega_r = 150 \text{ rad/sec}$.

The sustain oscillation are obtained at the gain value of $K_{psmax} = 60$ & $K_{pimax} = 25$ and ultimate period of P_u has been observed equal to 0.2 sec as shown in Fig. 4. Now the controller gain is adjusted by Ziegler Nichols method, first for P controller. The steady state condition is reached with $K_{ps} = 30$ & $K_{pi} = 12.5$ as shown in Fig. 5. It is clear that time to reach steady state value is approximately 1.2 sec.

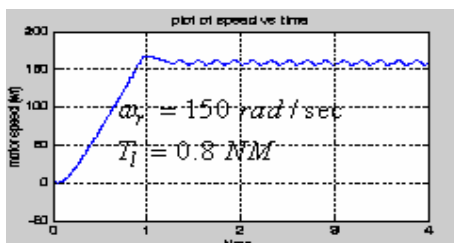


Fig. 4. Plot of rotor speed (ω_r) vs time (t)

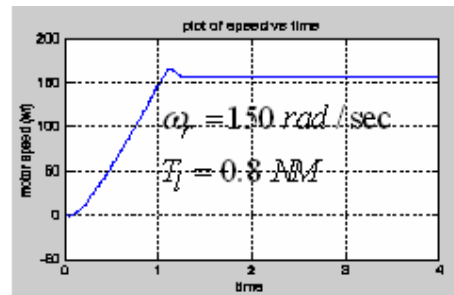


Fig. 5. Plot of rotor speed (ω_r) vs time (t) with P controller

Next the controller gain is adjusted for PI controller and in this case the steady state condition is reached with $K_{ps} = 27$ & $K_{pi} = 11.25$ as shown in Fig. 6. The time to reach steady state speed is approximately 1.3 sec in this case. Since with P controller there is no offset thus with PI controller system become sluggish as desired.

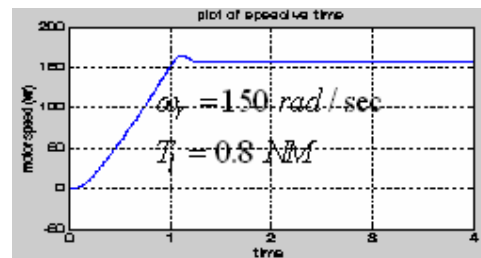


Fig. 6. Plot of rotor speed (ω_r) vs time (t) with PI controller

The load torque is now increased gradually and it has been observed that up to a value of 4 Nm same controller gain value works satisfactorily as shown in Fig. 7, Fig. 8 and Fig 9 for sustain oscillation, P controller, and PI controller respectively. It is observed that if the load torque is increased, the DC link current range increases to obtain the steady state operating value. This reduces the time to reach the steady state speed as shown in Fig. 8 and Fig. 9. The DC link current taken by the CSI inverter with $T_l = 0.8 \text{ Nm}$ is approximately 8 amps as shown in Fig. 10 and it reaches to 22 amps for a load torque of 4 Nm shown in Fig. 11.

These controller values work satisfactorily up to a torque of 18 Nm.

When the speed of the motor is reduced say, $\omega_r = 145 \text{ rad/sec}$ then for the same initial load torque of $T_l = 0.8 \text{ Nm}$ the sustain oscillation are now obtained at the gain value of $K_{psmax} = 38$ and $K_{pimax} = 20$ and ultimate period of $P_u = 0.203 \text{ sec}$ as shown in Fig. 12. The speed transients for P controller and PI controller are shown in Fig. 13 and Fig. 14, respectively for this starting load torque. These gain values are constant if the load torque is increased up to a value of 4 Nm as shown in Fig. 15, Fig. 16 and Fig. 17 for sustain oscillations, P controller and PI controller respectively.

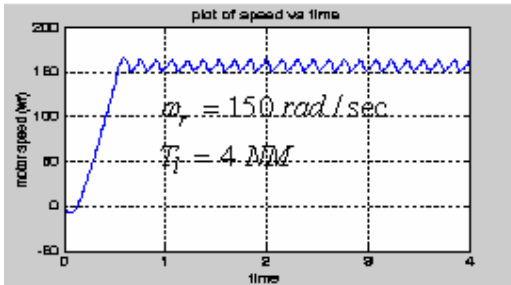


Fig. 7. Plot of rotor speed (ω_r) vs time (t)

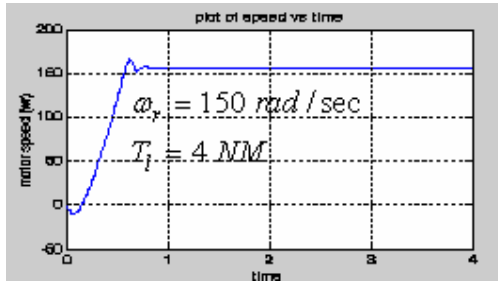


Fig. 8. Plot of rotor speed (ω_r) vs time (t) with P controller

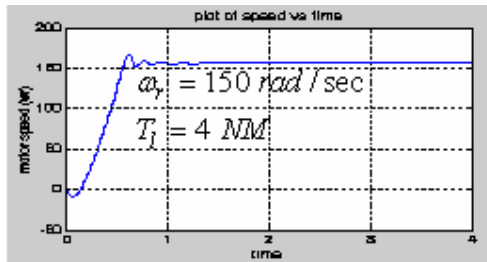


Fig. 9. Plot of rotor speed (ω_r) vs time (t) with PI controller

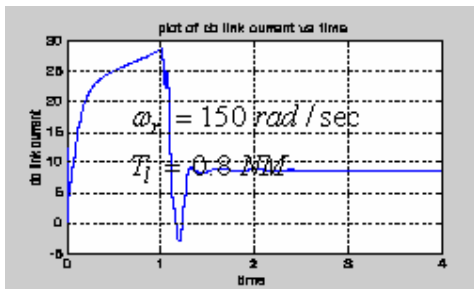


Fig. 10 Plot of dc link current (i_{dc}) vs time (t) with P controller

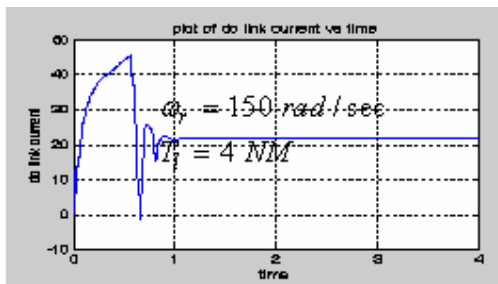


Fig. 11 Plot of dc link current (i_{dc}) vs time (t) with PI controller

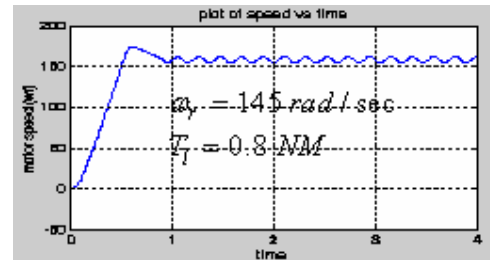


Fig. 12. Plot of rotor speed (ω_r) vs time (t)

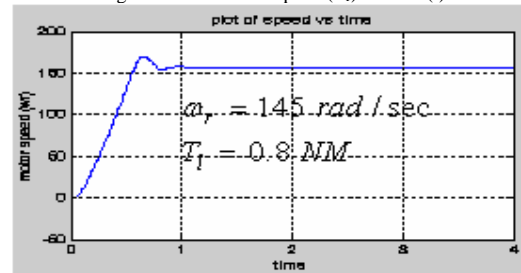


Fig. 13. Plot of rotor speed (ω_r) vs time (t) with P controller

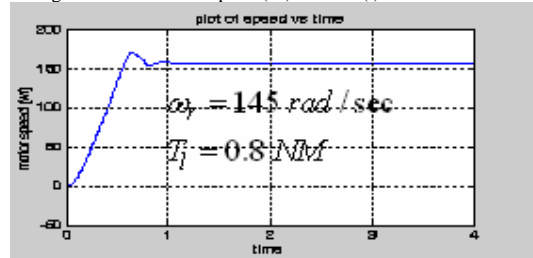


Fig. 14. Plot of rotor speed (ω_r) vs time (t) with PI controller

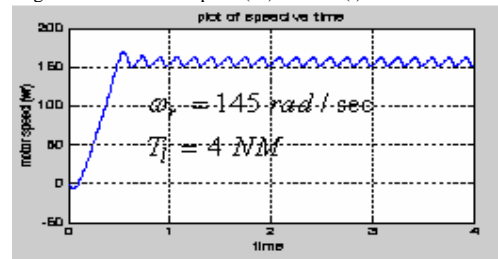


Fig. 15. Plot of rotor speed (ω_r) vs time (t)

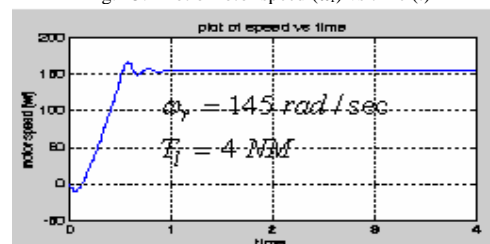


Fig.16. Plot of rotor speed (ω_r) vs time (t) with P controller

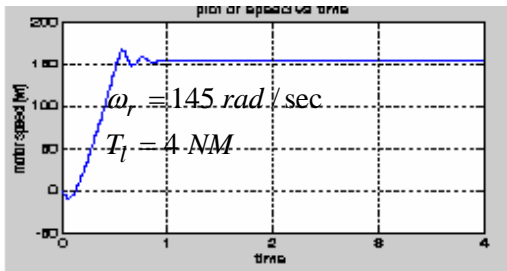


Fig. 17. Plot of rotor speed (ω_r) vs time (t) with PI controller

It has also been observed that with a reduction in speed the corresponding DC link current range is reduced. The DC link current taken by the CSI inverter with $\omega_r = 150 \text{ rad/sec}$ and $T_l = 0.8 \text{ Nm}$ was approximately 8 amps (Fig. 10) but with increasing speed error and with same load torque DC link current has become approximately 6.8 amp as shown in Fig. 18. This reduction in DC link current reduces the transient time of the system which can be observed in Fig. 12 as compared to Fig. 5

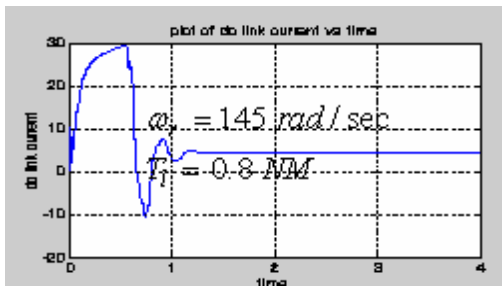


Fig. 18 Plot of dc link current (i_{dc}) vs time (t) with P controller

VI. CONCLUSIONS

Mathematical modeling of current source inverter (CSI) fed induction motor drive system has been done in synchronously rotating d-q reference frame using proportional and integral regulators in speed and current loops. Tuning of speed controller and current controller is performed using simulation in MATLAB in DTC approach. A capacitor bank is mounted on the terminal of drive for maintaining better power factor at each operating condition of the drive. The steady-state parameters and slip regulator characteristics of the drive are determined experimentally. Steady state and Transient performance are obtained by developing a computer program. A number of observations have been made to analyze various waveforms. Motor has been loaded with rated load. Optimum value of controller parameters is determined by Ziegler and Nichols method for different motor speed. It has been found that for low value of torque without any controller sustained oscillation are obtained and ultimate period of P_u has been observed equal to 0.2 sec. However, with P and PI controllers these oscillations are almost zero and the time to reach steady state value is approximately 1.2 sec for P controller and 1.3 sec for PI controller. Since with P controller there is no offset thus with PI controller system become sluggish as desired.

The controller constants remain same for increase of load torque but the DC current requirement increases which results the reduction in settling time.

The controller constants reduce with a decrease in speed and at the same time the DC link current requirement also decreases. This again increases the system stability.

VII. REFERENCES

- [1] T.A Lipo, "Recent progress in the development of solid state ac motor drives", IEEE Trans Power Electronics, Vol. PE-3, pp 105-117, April 1988.
- [2] M. Hombu, S. Ueda and A. Ueda, "A current source GTO Inverter with sinusoidal inputs and outputs", IEEE Trans. on. Industrial .Application, Vol. IA /23, pp. 247-255, March/April 1987.
- [3] Bin Wu, Shashi B. Dewan and Gardon R. Slemon, "PWM CSI Inverter for Induction Motor Drives", IEEE Transactions on Industry Applications, Vol.28, No.1, January/February 1992.
- [4] B.K. Bose, "Adjustable speed ac drives", A technology status review, Proc. IEEE, Vol. 70, pp. 116-135, Feb 1982.
- [5] Ajit K Chattopadhyay, "Current Source Inverter Fed Induction Motor Drives A state of the Art Research Review", JIE , Vol. 37, pp-34-46, 1991.
- [6] S. Nonaka and Y. Neba, "New GTO current source Inverter with pulse width modulation control Technique", IEEE Trans. Industrial Application. Vol. IA /22, pp. 666-672, July/Aug. 1986.
- [7] Jose R. Espinoza and Geza Joos, "A Current Source Inverter fed Induction Motor Drive system with Reduced Losses", IEEE Transactions on Industry Applications, Vol.34, No.4, July/August 1998.
- [8] M. K. Sang, Y. H. Woo and G. L Chang., "Improved Self-tuning Fuzzy PID Controller for Speed Control of Induction Motor", IEEJ Trans. IA, Vol.124, No.7, 2004.
- [9] M. Nasir Uddin and Hao Wen, "Development of a Self-Tuned Neuro-Fuzzy Controller for Induction Motor Drives", Industry Application Conference, 2004, 39th IAS Annual Meeting Conference Record of the 2004 IEEE, Vol. 4, 3-7 Oct. 2004 Page(s): 2630-2636.
- [10] Abdul Rahiman, Beig, and V. T. Ranganathan, "A Novel CSI-Fed Induction Motor Drive", IEEE Trans. On Power Electronics, Vol. 21, No.4, July 2006.
- [11] M. Zerikat, M.Benjebbar and N. Benouzza, "Dynamic Fuzzy-Neural Network Controller for Induction Motor Drive", Transaction on Engineering, Computing and Technology, Dec-2005, ISSN 1305-5313.
- [12] Peter Harriott, "Process Control", Tata McGraw-Hill Publishing Company Limited New Delhi.
- [13] Piush. Kumar, and Vineeta Agarwal, "A Model for Current Source Inverter Fed Induction Motor", Journal of Electrical & Electronics System Research, Vol.1, June 2008.

VIII. BIBLIOGRAPHIES



Piush Kumar graduated from Karnataka University Dharwad India, with Electrical and Electronics Engg in 1998 and received his Master's degree in 2003, from M.M.M. Engg College Gorakhpur. He is pursuing his PhD from Motilal Nehru National Institute of Technology, Allahabad, India.



Vineeta Agrawal graduated from Allahabad University, India, in 1980, and received her Master's degree in 1984, from the same university. She joined as lecturer in 1982 in Electrical Engineering Department in M. N. R. Engineering College. While teaching, she did her Ph.D. course in Power Electronics. At present she is Professor in the Department of Electrical Engineering at Motilal Nehru National Institute of Technology, Allahabad. She is senior member of IEEE. She has taught numerous courses in Electrical and Electronics. Her research interests are in single phase to three-phase conversion and AC drives. She has a number of publications in Journals and Conferences in her field. She has attended both National and International Conferences and presented papers there.